DINAME 2017 - Proceedings of the XVII International Symposium on Dynamic Problems of Mechanics
A. T. Fleury, D. A. Rade, P. R. G. Kurka (Editors), ABCM, São Sebastião, SP, Brazil, March 5-10, 2017

Stability Diagnosis for Rotor–Seal System by Utilizing Active Magnetic Bearing

Wataru Tsunoda[1], Christian Wagner[2], Tobias Berninger[2], Thomas Thuemmel[2] and Daniel Rixen[2]

[1] Department of Mechanical Engineering, Tokyo Institute of Technology, 4259, Nagatsuta-cho, Midori-ku, 226-8503 Yokohama, Japan, tsunoda.w.aa@m.titech.ac.jp

[2] Chair of Applied Mechanics, Technical University of Munich, Boltzmannstrasse 15, 85748 Garching, Germany, c.wagner@tum.de, t.berninger@tum.de, thuemmel@tum.de, rixen@tum.de

Abstract: Rotational machinery usually pressurizes or compresses fluid in a plenum. However, a seal, which prevents a leakage of liquid from a plenum, causes self-excited vibration due to the cross-coupled stiffness at a high rotational speed, and then the instability leads to a breakdown of the system. Thus, a stability diagnostic method is necessary for the stable and safety operation. On the other hand, an active magnetic bearing (AMB) has a superior controllability to other bearings, although it does not have a large load carrying capacity. Recently, excitation by active magnetic bearings to diagnose stability has been proposed, and most of them have focused on measuring coefficients of seals. On the other hand, the purpose of this research is to diagnose the stability by estimating the rotational speed at which self-excited vibration occurs by utilizing an active magnetic bearing. This method is experimentally evaluated with our test rig.

Keywords: Dynamics of rotating bodies, Liquid annular seal, Active magnetic bearing, Self-excited vibration, Stability diagnosis

NOMENCLATURE

Latin symbols

M : mass
C : direct damping
c : cross-coupled damping
K : direct stiffness
k : cross-coupled stiffness
F : external force
j : imaginary unit
s: Laplace operator
z : forward whirl coordinate
$\dot{z}$: velocity of z
$\ddot{z}$: acceleration of z

Greek symbols

Ω : rotational speed
λ : ratio between C and k
ν : excitation frequency

Subscripts

x, y, z : relative to coordinates
re0, im0: real part and imaginary part become zero
onset : onset

INTRODUCTION

Rotational machinery such as compressors and turbopumps usually pressurizes or compresses fluid in a plenum. However, a seal, which prevents a leakage of liquid from a plenum, causes self-excited vibration due to the cross-coupled stiffness at a high rotational speed, and then the instability leads to a breakdown of the system. Moreover, a condition of a rotor system changes during long-term operation. Thus, a stability diagnostic method is necessary for the stable, safety and long-term operation.

The authors have developed the stability diagnostic method for a rotor-oil film bearing system (Matsushita and Fujiwara, 2014, Tsunoda et al., 2016). The rotor supported by oil film bearings also has the instability such as oil whip and oil whirl at a high rotational speed. Our method is to predict the onset rotational speed at which the self-excited vibration occurs by utilizing an active magnetic excitation. An active magnetic bearing (AMB) has a superior controllability to other bearings, although it does not have a large load carrying capacity. The mechanisms of the instabilities of oil film bearing nearly equal to that of seal, so we evaluated the possibility to apply our diagnostic method of oil film bearing to the seal instability.

Previous researches have also utilized an excitation of active magnetic bearings to diagnose stability, and most of them have focused on measuring coefficients of seals (Kwanka, 1999, Zutavern, 2006, Wagner, 2016). On the other hand, the purpose of this research is to diagnose the stability by estimating the rotational speed at which self-excited vibration occurs.

In this paper, first, a method for estimating the speed at which self-excited vibration occurs is proposed by considering both the Bently/Muszynska (B/M) model (Muszynska, 1986, Bently et al., 2002) and a reduced-order rotor/shaft model utilizing the Jeffcott-rotor model. Then, the proposed diagnostic method is experimentally evaluated.

TEST RIG

Figure 1 shows a photograph and a schematic view of the experimental test rig. Table 1 describes the main dimensions. In the test rig, the rotor is supported by ball bearings at the both ends and the rotor has a mass disk at the center of the shaft. The mass disk has two seals at the ends of the disk, where the pressurized oil is injected. An AMB is placed between the ball bearing and the seal to excite the rotor. The rotor displacement is measured by eddy current type displacement sensors (U1, MICRO-EPSILON). The maximum rotational speed is 100 rps. The natural frequency of the 1st dry bending mode 38.6 Hz is measured by an impact hammer testing without the seals.

The waterfall plot of the displacement at the mass disk is shown in Fig. 2. The test rig does not have a critical speed because the high damping effect of the seals makes the rotor the overdamped system. The large peak in the figure indicates the unbalance response. The rotor, moreover, has a small response at the half-rotational speed. This response indicates the natural frequency of the rotor. Due to the speed limitation of the motor, the instability does not appear in Fig. 2. Therefore, the onset speed is numerically calculated in the next section.

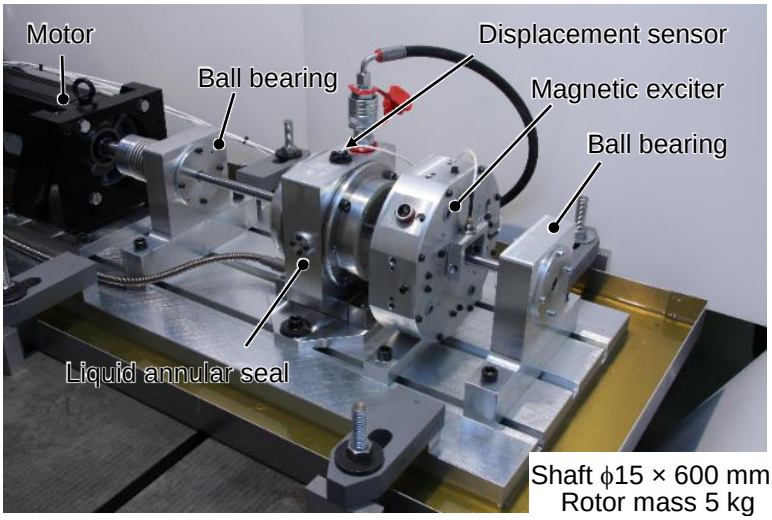

(a) Photograph

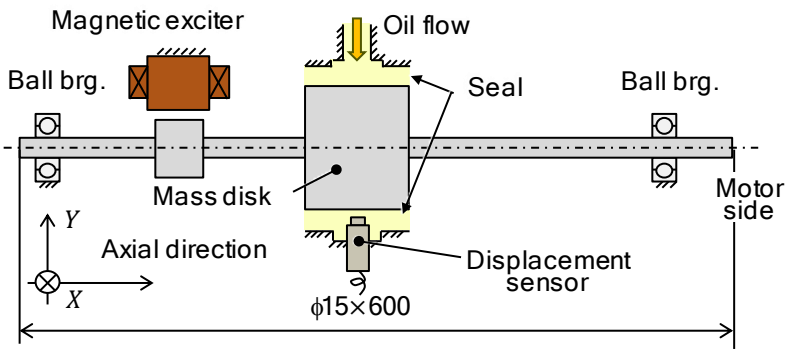

(b) Schematic view

Figure 1 - Test rig

Table 1 - Dimensions and parameters of test rig

	Name	*Value*		*Name*	*Value*
Seal	Length	20 [mm]	AMB	Inner diameter	47.8 [mm]
	Diameter	100 [mm]		Pole area	218 [mm^2]
	Clearance	0.17 [mm]		Clearance	0.5 [mm]
	Pressure	200 [kPa]		Hetero type, 8 poles	
	Viscosity	0.0391 [Pa·s]	Rotor	Shaft	ϕ15×600 [mm]
				Mass	5 [kg]
				Natural freq. of 1st bending mode	38.6 [Hz]

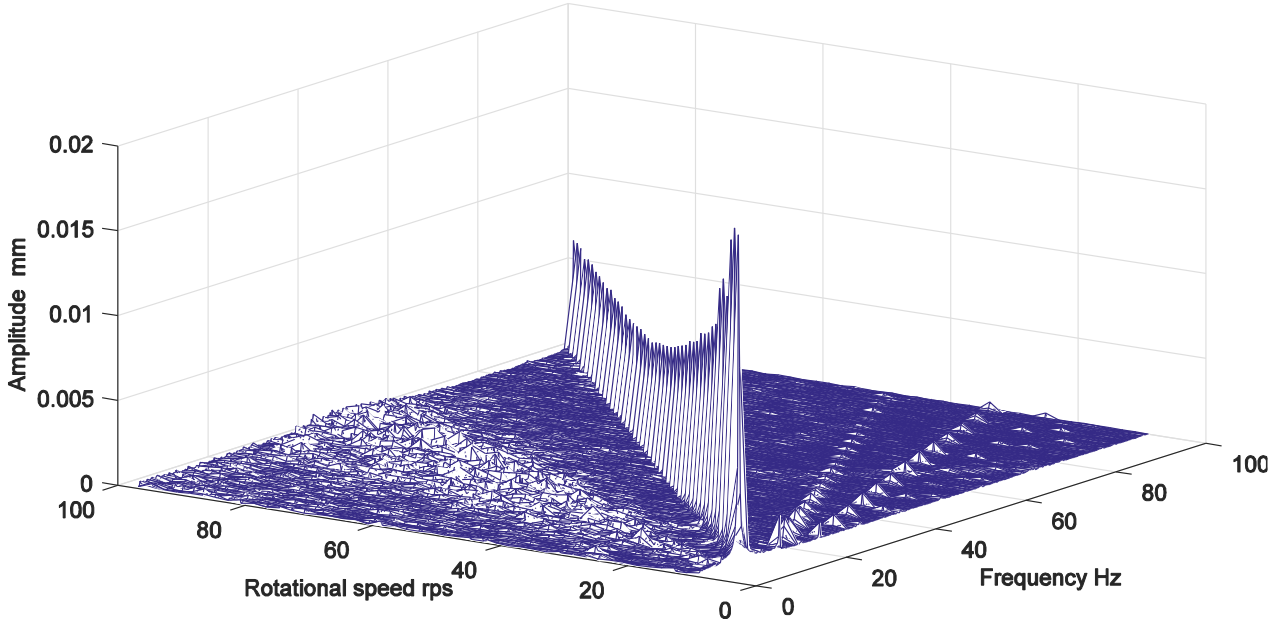

Figure 2 - Waterfall plot of the rotor displacement

ROTOR MODEL AND SEAL MODEL

We modeled the test rig with the Jeffcott-rotor model, which neglects the mass of the rotor shaft (Gasch, 2002). The liner rotor model is shown in Fig. 3. The rotor mass is directly supported by the shaft and the seals. The rotor displacement is defined as $[x \;\; y]^{\mathrm{t}}$. The equation of motion in the model is described as follows:

$$\begin{bmatrix} F_{\mathrm{x}} \\ F_{\mathrm{y}} \end{bmatrix} = \begin{bmatrix} M_{\mathrm{r}} + M_{\mathrm{s}} & 0 \\ 0 & M_{\mathrm{r}} + M_{\mathrm{s}} \end{bmatrix} \begin{bmatrix} \ddot{x} \\ \ddot{y} \end{bmatrix} + \begin{bmatrix} C_{\mathrm{s}} & c_{\mathrm{s}} \\ -c_{\mathrm{s}} & C_{\mathrm{s}} \end{bmatrix} \begin{bmatrix} \dot{x} \\ \dot{y} \end{bmatrix} + \begin{bmatrix} K_{\mathrm{r}} + K_{\mathrm{s}} & k_{\mathrm{s}} \\ -k_{\mathrm{s}} & K_{\mathrm{r}} + K_{\mathrm{s}} \end{bmatrix} \begin{bmatrix} x \\ y \end{bmatrix} \tag{1}$$

where $M_{\mathrm{r}} = 5$ [kg] is the rotor mass, $K_{\mathrm{r}} \approx 2.9{\times}10^5$ [N/m] is the coefficient of the shaft stiffness and M_{s}, C_{s} and K_{s} are the coefficients of the direct mass, damping and stiffness of the seals, respectively. c_{s} and k_{s} are the coefficients of the cross-coupled damping and stiffness. We assume that the cross-coupled mass of the seal is so small to neglect it and the rotor does not have anisotropic effect. In the case of the isotropic rotor, the instability causes in the forward whirl direction, thus, we focus on only the forward direction. The equation of the motion in the forward direction is shown below with the forward whirl coordinate $z = x + jy$.

$$F_z = M\ddot{z} + C\dot{z} - jc\dot{z} + Kz - jkz \tag{2}$$

where M, K C, c and k are $M_{\mathrm{r}} + M_{\mathrm{s}}$, $K_{\mathrm{r}} + K_{\mathrm{s}}$ C_{s}, c_{s} and k_{s}, respectively.

Next, we numerically calculate the seal coefficients for eigenvalue analysis. By utilizing the Childs model (Childs, 1983), we numerically solve the Bulk-flow model and obtain the coefficients of the seal. The calculated

coefficients are shown in Fig. 4, where the coefficients of the damping are multiplied by the rotational speed Ω. The coefficients of the direct stiffness K is almost constant at less than 60 rps and then that decreases at higher rotational speed than 60 rps. The cross-coupled damping $c\Omega$ is proportion to the square of the rotational speed. The coefficients of the direct damping $C\Omega$ and the cross-coupled stiffness k are almost proportion to the rotational speed. The ratio between $C\Omega$ and k is defined as λ, which is almost 0.5. By substituting $k = C\lambda\Omega$ into Eq. (2), we obtain the following equation.

$$F_z = M\ddot{z} - jc\dot{z} + Kz + C\dot{z} - jC\lambda\Omega z \tag{3}$$

This seal model is called as B/M model.

The calculated eigenvalues are shown in Fig. 5. These values are calculated by solving the characteristic equation of Eq. (3). The real part of the eigenvalue becomes positive value at 116 rps. Therefore, the calculated onset rotational speed is 116 rps.

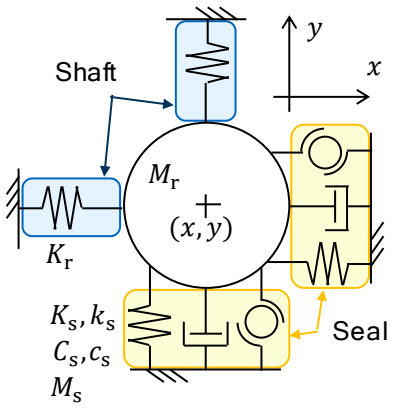

Figure 3 - Rotor model

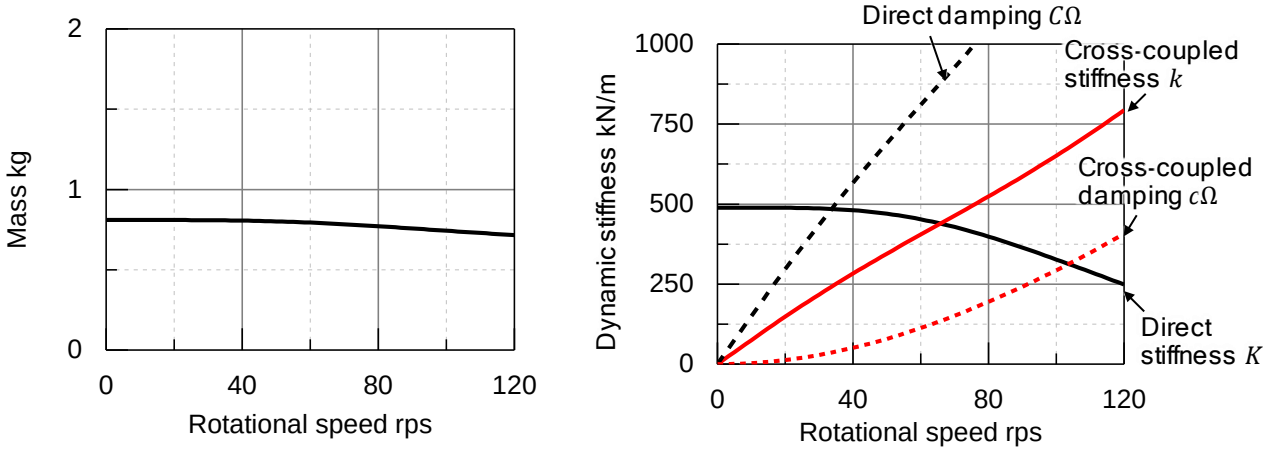

Figure 4 - Calculated coefficients

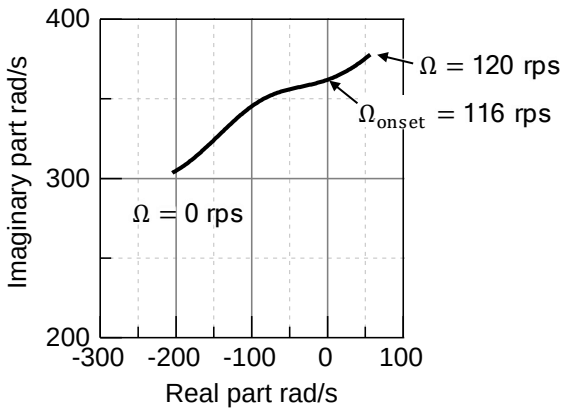

Figure 5 - Calculated eigenvalue in root locus plot

ANALITICAL INVESTIGATION ON STABILITY LIMIT

The eigenvalues change with the rotational speed because the coefficients have different values at each rotational speed. Based on the FFT result in Fig. 2, the rotor has the natural frequency at half of the rotational speed. The instability usually occurs at the half speed frequency, which is the natural frequency of the system. Therefore, the eigenvalue of the rotor system can be described as $s = j\lambda\Omega + \Delta s$, where Δs indicates the real part of the eigenvalue. We substitute $s = j\lambda\Omega + \Delta s$ into the characteristic equation of Eq. (3), and then we derive the following equation.

$$M(j\lambda\Omega + \Delta s)^2 - jc(j\lambda\Omega + \Delta s) + K - C\Delta s = 0 \tag{4}$$

Δs is small enough to neglect Δs^2. Thus, we simplify it as the next.

$$-M(\lambda\Omega)^2 + c\lambda\Omega + K + (2jM\lambda\Omega - jc - C)\Delta s = 0 \tag{5}$$

C is usually much larger than the other coefficients of Δs, so M and c in the last turms are neglected as follows;

$$-M(\lambda\Omega)^2 + c\lambda\Omega + K - C\Delta s = 0 \tag{6}$$

The condition of the stability limit $\Delta s = 0$ is shown below.

$$-M(\lambda\Omega)^2 + c\lambda\Omega + K = 0 \tag{7}$$

Therefore, if we predict the condition at which Eq. (7) is satisfied, the onset speed Ω_{onset} can be predicted. We propose the measurement method of the condition of stability limit in the next section.

PREDICTION METHOD OF ONSET SPEED

The test rig has a magnetic exciter, and we apply the sweep excitation in the forward direction at the excitation frequency ν. In order to calculate the rotor response, $s = j\nu$ is substituted into the Laplace transformed Eq. (3). The transfer function of the rotor-seal system is shown as the next equation.

$$\frac{z}{F_z} = \frac{1}{-M\nu^2 + c\nu + K + jC(\nu - \lambda\Omega)} \tag{8}$$

The real part and imaginary part of Eq. (8) are calculated as follows:

$$\mathrm{Re}\left(\frac{z}{F_z}\right) = \frac{-M\nu^2 + c\nu + K}{(-M\nu^2 + c\nu + K)^2 - \{C(\nu - \lambda\Omega)\}^2} \tag{9}$$

$$\mathrm{Im}\left(\frac{z}{F_z}\right) = \frac{-C(\nu - \lambda\Omega)}{(-M\nu^2 + c\nu + K)^2 - \{C(\nu - \lambda\Omega)\}^2} \tag{10}$$

The zero-crossing frequency of the real part ν_{re0}, for which Eq. (9) is equal to 0, is derived as the next.

$$-M\nu_{\mathrm{re0}}^2 + c\nu_{\mathrm{re0}} + K = 0 \tag{11}$$

The zero-crossing frequency of the imaginary part ν_{im0}, for which Eq. (10) is equal to 0, is derived as the next.

$$\nu_{\mathrm{im0}} = \lambda\Omega \tag{12}$$

When the zero-crossing frequency of the real part ν_{re0} become the same value with that of the imaginary part ν_{im0} at a high rotational speed, the stability limit as shown in Eq. (7) is satisfied, then the self-excited vibration occurs. Figure 6 shows the zero-crossing frequencies of ν_{re0} and ν_{im0}. ν_{im0} is almost proportion to the rotational speed because λ is around 0.5. On the other hand, ν_{re0} also changes with the rotational speed. The cross section of the fitted lines should indicate the onset rotational speed because ν_{re0} equals to ν_{im0} at Ω_{onset}. In order to measure the zero-crossing frequencies, we utilize the co-quad analysis method, which separates the transfer function into the real and imaginary part explained in the next section.

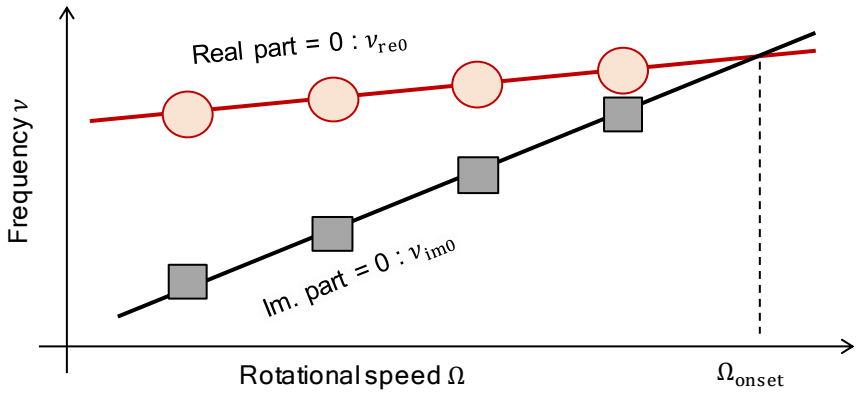

Figure 6 – Concept of the proposed estimation method of onset speed

EXPERIMENTAL EVALUATION OF THE PROPOSED ONSET ESTIMATION METHOD

Experimental Set Up for Estimating the Onset

Figure 7 shows a block diagram for measuring the rotor response caused by magnetic excitation. The upper part of the DSP system (ds1103, dSPACE GmbH) shows the signal generator for the reference coil-current. The coil-current is supplied by the power amplifiers to the electromagnets. The coil-current of cosine wave is supplied into the X directional coil, and that of sine wave is for the Y direction. The coil inductance could cause the phase delay, thus, we measured the phase delay from the reference coil-current to the actual coil-current. The measured phase delay is less than 1 degree at $\nu = 100$ Hz, so we can neglect the phase delay.

The bottom part shows the co-quad analysis algorithm, which calculates the values of the real and imaginary parts of the frequency response. The response is multiplied by the referential signals, then that is multiplied by the low pass filter and the gain 2. This method can calculate the real and imaginary parts of the transfer function in real time. The evaluation tests are carried out at 30, 50, 70, 90 and 100 rps with the amplitude of the coil current set to 1 A. According to a pre-testing, 1 A of coil-current generates around 70 N with the rotor centralized. Excitation frequency is from 15 to 120 Hz.

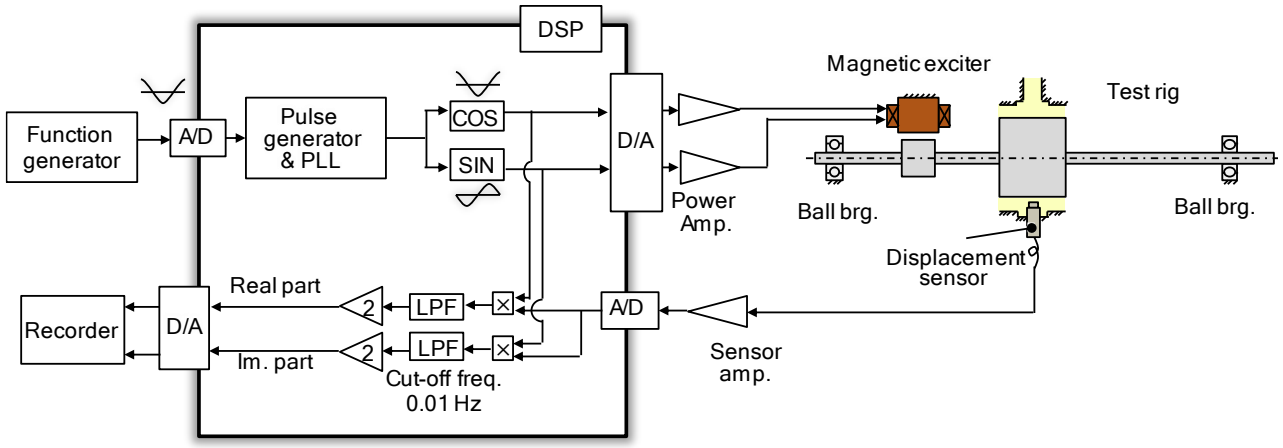

Figure 7 - Block diagram for the proposed diagnosis

Experimental Results of the Onset Estimation

Figure 8 shows the co-quad analysis results measured at 90 rps. The real part shown in the black line becomes zero at 61.3 Hz. Therefore, we obtain $\nu_{re0} = 61.3$ Hz. The red line cross zero at 43.7 Hz, so $\nu_{im0} = 43.7$ Hz. In the same way, we measured the zero-crossing frequencies at the other rotational speed.

The zero-crossing frequencies measured at 30, 50, 70, 90 and 100 rps are shown in Fig. 9. The red dots indicate the zero-crossing frequencies of the real part ν_{re0}. They are around 60 Hz at all rotational speed range. The black dots show those of the imaginary part ν_{im0}, which are proportion to the rotational speed. The proportional ratio is about 0.5. The liner fitted lines have the cross section at 121 rps. Our estimated onset speed agrees well with the simulated onset speed 116 rps.

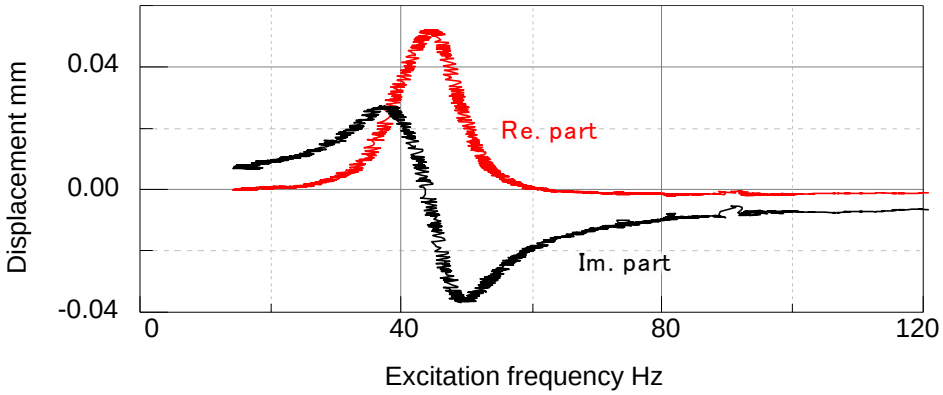

Figure 8 – Co-quad analysis results measured at 90 rps;
The red line and black line show the real and imaginary parts, respectively

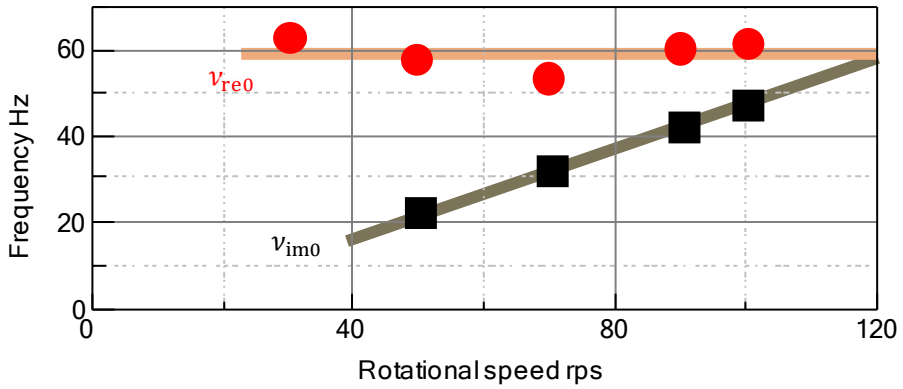

Figure 9 – Zero-crossing frequencies;
the estimated onset rotational speed is 121 rps

CONCLUSION

A method for diagnosing the stability of rotor-seal systems is proposed. The method estimates the rotational speed at which self-excited vibration occurs. A theoretical explanation of the method is given by considering the B/M model and a 1 DOF Jeffcott-rotor model. In this method, the frequency response due to magnetic excitation is measured and analyzed by co-quad analysis, and then ν_{re0} and ν_{im0} are obtained from zero-crossing frequencies to estimate the onset speed. The estimated onset of 121 rps is approximately equal to the calculated onset of 116 rps. In future work we will increase the maximum rotational speed of our test rig and then compare the actual onset rotational speed to the estimated onset speed.

REFERENCES

Bently, D., E., Hatch, C., T. & Grissom, B., 2002, Fundamentals of Rotating Machinery Diagnostics (Design and Manufacturing), Bently Pressurized Bearing Press, pp. 475- 497.

Childs, D. W., 1983, Dynamic Analysis of Turbulent Annular Seals Based On Hirs Lubrication Equation. Journal of Lubrication Technology, Vol. 105, pp. 429-436

Gasch, R., Nordmann R. and Pfuetzner, H., 2002, Rotordynamik. Springer.

Kwanka, K., 1999, Dynamic Coefficients of Stepped Labyrinth Gas Seals, ASME 1999 International Gas Turbine and Aero Engine Congress and Exhibition, Indiana, USA.

Matsushita, O. and Fujiwara, H., 2014, Rotordynamics in HIL and Vibrational diagnostic technics, *v_BASE* forum 2014, Tokyo, Japan.

Muszynska, A., 1986, Whirl and Whip –Rotor/Bearing Stability Problems-, Journal of Sound and Vibration, Vol. 110, No. 3, pp. 443- 462.

Tsunoda. W., Hijikata, W., Shinshi, T., Fujiwara, H. and Matsushita, O., 2016, Diagnostic experiments for stability of rotor-oil film bearing systems using radial magnetic bearing excitation, Vibrations in Rotating Machinery (VIRM 11), Manchester, UK.

Zutavern, Z. S., 2006, Identification of rotordynamic forces in a flexible rotor system using magnetic bearings, Doctor Thesis, Texas A&M University.

Wagner, C., Berninger, T., Thümmel, T. and Rixen D., 2016, Rotordynamic Effects in Turbopumps, Space Propulsion 2016 Conference, Rome, Italy.

RESPONSIBILITY NOTICE

The authors are the only responsible for the material included in this paper.